ACS APPLIED MATERIALS & INTERFACES

Research Article

www.acsami.org

Magnetic Properties of bcc-Fe(001)/C_{60} Interfaces for Organic Spintronics

T. Lan Anh Tran,[†] Deniz Çakır,[‡] P. K. Johnny Wong,[†] Alexei B. Preobrajenski,[§] Geert Brocks,[‡] Wilfred G. van der Wiel,[†] and Michel P. de Jong*[,†]

[†]NanoElectronics Group, MESA+ Institute for Nanotechnology, University of Twente, P.O. Box 217, 7500 AE Enschede, The Netherlands

[‡]Computational Materials Science, Faculty of Science and Technology and MESA+ Institute for Nanotechnology, University of Twente, P.O. Box 217, 7500 AE Enschede, The Netherlands

[§]MAX-lab, Lund University, Box 118, 22100 Lund, Sweden

ABSTRACT: The magnetic structure of the interfaces between organic semiconductors and ferromagnetic contacts plays a key role in the spin injection and extraction processes in organic spintronic devices. We present a combined computational (density functional theory) and experimental (X-ray magnetic circular dichroism) study on the magnetic properties of interfaces between bcc-Fe(001) and C_{60} molecules. C_{60} is an interesting candidate for application in organic spintronics due to the absence of hydrogen atoms and the associated hyperfine fields. Adsorption of C_{60} on Fe(001) reduces the magnetic moments on the top Fe layers by ∼6%, while inducing an antiparallel magnetic moment of ∼−0.2 μ_B on C_{60}. Adsorption of C_{60} on a model ferromagnetic substrate consisting of three Fe monolayers on W(001) leads to a different structure but to very similar interface magnetic properties.

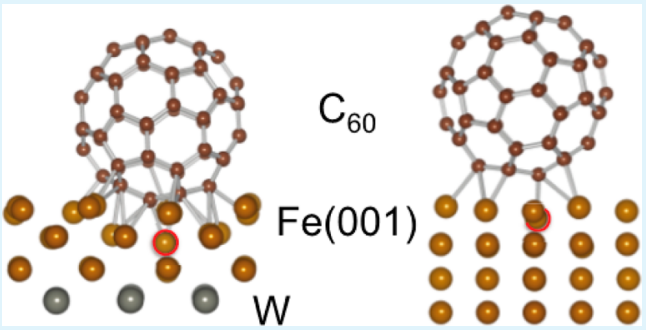

KEYWORDS: *metal−organic interfaces, spintronics, X-ray absorption spectroscopy, X-ray magnetic circular dichroism, first-principles calculations, density functional theory*

INTRODUCTION

Organic semiconductor spintronics, which focuses on information processing via charge carrier spins in carbon-based, molecular semiconductors, is a new and exciting field of nanoelectronics.[1,2] Organic semiconductors (OSCs) are suitable hosts for spin polarized carriers, because the spin-orbit coupling and hyperfine interactions in these materials are relatively weak. This leads to long spin relaxation and dephasing times (>1 μs) compared to those attainable in inorganic semiconductors, which in principle allows for robust spin operations and read-out.[2,3]

Large magnetoresistance (MR) effects have been observed in vertical organic spin valves, where OSCs are sandwiched between two ferromagnetic (FM) electrodes, and are used either as a tunnel barrier[4−6] or as charge/spin transport medium.[5,7] Substantial MR at room temperature has been reported in spin valves based on tris(8-hydroxy-quinolinato) aluminum (Alq3)[4,5,7−9] and on C_{60}.[6,10−12]

Phenomenological models for the observed magnetotransport effects have been developed,[5,9] yet the microscopic physical mechanisms remain poorly understood. It has become clear that the electronic structure, in particular the spin polarization, of the hybrid interfaces between the OSC and the ferromagnetic metal electrodes, plays a key role in spin injection and spin extraction.[5] Consequently, an important obstacle in developing a microscopic understanding of these processes is formed by the challenge of fabricating devices with electronically, magnetically, and structurally well-defined hybrid interfaces.

Incorporating such well-defined interfaces into organic spintronic devices would allow for a direct comparison with theoretical modeling and is therefore of great importance to advance the understanding of the operation mechanisms of these devices. Furthermore, systematic studies of various relevant OSC/FM interfaces are required to exploit the full potential of *tailoring* the interfacial spin polarization via hybridization effects, an approach that has been coined "spinterface science".[13] Such spin dependent hybridization can give rise to large magnetoresistance effects, as has been shown recently by scanning tunneling microscopy experiments.[14]

Here, we present a combined computational and experimental study on the magnetic properties of interfaces between bcc-Fe(001) and C_{60} for organic spintronic devices. Fullerenes

Received: October 23, 2012
Accepted: January 10, 2013
Published: January 10, 2013

such as C_{60} are particularly interesting candidates for application in organic spintronic devices, due to the absence of hydrogen atoms which give rise to spin dephasing via hyperfine interactions. C_{60} layers can be grown in a controlled way on a bcc-Fe(001) substrate.[15] An important issue that we wish to address is the impact of the C_{60}/Fe interaction on the spin polarization at the interface. Similar to the case of C_{60} on Cr(001),[16] a significant chemical interaction is expected, which would lead to spin polarized hybrid states. We use first-principles density functional theory (DFT) calculations to extract the magnetizations of the Fe surface and of the C_{60}/Fe interface.

Carbon *K-edge* X-ray absorption spectroscopy (XAS) and X-ray magnetic circular dichroism (XMCD) measurements of C_{60} layers on Fe(001) indicate a sizable spin polarization of the unoccupied C_{60} states just above the Fermi level, induced by the interaction with the Fe substrate.[15] A similar Fe $L_{2,3}$ edge XAS/XMCD analysis of the interaction induced changes in the spin polarization of the Fe surface atoms is hampered by the significant contribution of the Fe bulk substrate to the XAS yield. To alleviate this problem, we use here an ultrathin Fe layer substrate, consisting of three Fe monolayers (ML) deposited onto a W(001) surface. In spite of the large experimental lattice mismatch of 10.4% between Fe and W, Fe grows pseudomorphically on W(001) at coverages below five ML.[17−19] A single Fe ML orders antiferromagnetically,[20,21] but a coverage of two or more ML leads to ferromagnetic ordering with in-plane anisotropy.[17−19] By means of DFT calculations, we study what extends the two substrates, Fe(001) and Fe/W(001), to lead to a difference in interaction with C_{60} molecules and to differences in the interface spin polarization.

COMPUTATIONAL RESULTS

The electronic and magnetic properties of the C_{60}/Fe(001) and C_{60}/Fe/W(001) interfaces are studied by DFT calculations using projector augmented wave (PAW) potentials and a plane wave basis set,[22,23] as implemented in the Vienna Ab initio Simulation Package (VASP).[24,25] Exchange and correlation are treated within the PBE formulation of the generalized gradient approximation (GGA).[26] Inclusion of van der Waals interactions is not necessary, as the interaction between Fe and C_{60} turns out to be chemisorption. We use a plane wave kinetic energy cutoff of 400 eV and a regular *k-point* grid with a spacing of 0.02 $Å^{-1}$ for the Brillouin zone sampling. We assume convergence when the difference of the total energies between two consecutive ionic steps is less than 10^{-5} eV and the maximum force allowed on each atom is 0.01 eV/Å. The calculated lattice constants of bulk bcc Fe and W are 2.83 and 3.17 Å, and the spin magnetic moment per atom of bulk Fe is μ_S = 2.20 μ_B, in good agreement with the experimental values of 2.87 and 3.16 Å and 2.22 μ_B.[27]

In agreement with previous studies, we find that the most stable magnetic order of a single Fe ML on W(001) is antiferromagnetic, whereas that of two or more Fe ML is ferromagnetic.[20,21,28] The calculated layer resolved μ_Ss of Fe(3 ML)/W(001) are given in Figure 1a (as the numbers between brackets). The enhancement of the surface μ_S, as compared to the bulk μ_S, is comparable to that in Fe(001). Not surprisingly, there is a difference in μ_S between the subsurface layers of Fe(001) and Fe/W(001), because of the proximity of the Fe/W interface. A small oscillating magnetization is induced in the W substrate. The interface W atoms have moments that are antiferromagnetically ordered with respect to the Fe overlayer, μ_S = −0.28 μ_B.[28] The moments in the subinterface W layers are at least an order of magnitude smaller.

We model the possible adsorption structures of one C_{60} ML on Fe(001) and Fe/W(001) substrates using a 4 × 4 surface unit cell containing one C_{60} molecule. The molecules are then arranged in a square lattice with a distance of 11.3 and 12.7 Å between neighboring

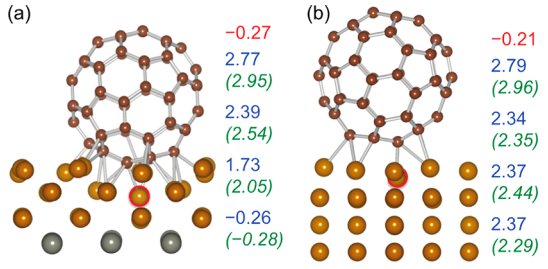

Figure 1. (a) C_{60}/Fe/W(001) structure viewed along the ⟨100⟩ direction. (b) C_{60}/Fe(001) structure viewed along the ⟨110⟩ direction. The numbers are the moments μ_S induced on the C_{60} molecules (red) and the layer averaged μ_S of the subsequent metal layers (blue). Between brackets are the layer resolved μ_S of the clean substrates.

C_{60} molecules, respectively, which is fairly close to the nearest neighbor distance of 10.1 Å in the fcc C_{60} crystal. The Fe(001) and Fe/W(001) substrates are modeled by slabs of 7 Fe ML and 3 Fe ML/5 W ML, respectively, with the C_{60} molecule absorbed on one side of the slab. A dipole correction is included to prevent spurious interactions between the repeated images of the slab. The top three Fe atomic layers, the W atomic layer at the interface, and the atoms of the C_{60} molecule are allowed to relax upon adsorption. The most favorable adsorption structure of C_{60} on the Fe surface is determined by relaxing a large number of possible adsorption structures.

The lowest energy structure of C_{60}/Fe(001) is shown in Figure 1b. The edge shared by two C_{60} hexagons (a double, or 6:6 bond) is on top of a surface Fe atom, indicated by a (red) circle. The C_{60} molecule is tilted such that one of the two edge-sharing hexagons is more parallel to the surface. Several Fe−C distances for C atoms in these two hexagons are in the range of 2.0−2.5 Å. The corresponding C−C distances are in the range of 1.46−1.52 Å, which is significantly larger than the 1.40 and 1.46 Å of the 6:6 and 5:6 bonds of isolated C_{60}. Only the structure of the C_{60} faces involving C atoms directly bonded to surface Fe atoms is modified, whereas the remaining faces are changed very little compared to isolated C_{60}. The calculated binding energy of C_{60} to the surface is 2.9 eV, which indicates a strong bonding, consistent with our previous experimental evidence for significant hybridization effects at C_{60}/Fe(001) interfaces.[15] Indeed, chemisorption of C_{60} is found for many metal substrates.[29,30]

One may expect a strained Fe lattice to be even more reactive, and the calculated binding energy, 4.1 eV, of C_{60} to Fe/W(001) confirms this. The larger in-plane lattice constant of Fe/W also allows for a stronger perturbation of the lattice upon adsorption of C_{60}, as shown in Figure 1a. The surface Fe atom below the 6:6 bond closest to the surface (marked by a red circle in Figure 1a) is pushed down into a row of the second Fe layer, and other Fe atoms relax as to maximize the bonding to C_{60}. Compared to adsorption on Fe(001), the C_{60} molecule sinks considerably deeper into the Fe/W(001) substrate. Note also that in the most favorable adsorption geometry the C_{60} molecule on the Fe/W substrate is rotated by 45° compared to its orientation on the Fe substrate.

The (layer averaged) moments μ_S of the C_{60}/Fe(001) and C_{60}/Fe/W(001) structures are also shown in Figure 1. In both these cases, the adsorption of C_{60} leads to a reduction of μ_S on the substrate Fe atoms. For adsorption on Fe(001), the average reduction of the surface Fe μ_S is 6%, and it drops to half that value in the third Fe layer. Within an Fe layer, the change in μ_S upon C_{60} adsorption is far from homogeneous. The surface Fe atom just below the 6:6 bond (marked in red in Figure 1b) has μ_S = 1.74 μB, which means a reduction of ∼40% compared to the clean Fe(001) surface.

The average reductions of μ_S of the top two Fe layers in C_{60}/Fe/W are comparable to those in C_{60}/Fe, i.e., ∼6%. Again, the changes are inhomogeneous. For instance, the Fe atom just below the 6:6 bond (marked in red in Figure 1a) has a much stronger reduced μ_S = 1.60 μ_B. As this atom is pushed into the second layer by C_{60} adsorption, it also perturbs the moments of the surrounding Fe atoms. Most remarkably, its largest perturbation is on its neighboring Fe atoms in

the third layer, where one of the atomic moments is even forced into antiparallel with $\mu_S = -1.19\ \mu_B$. The average μ_S of the third Fe layer is then reduced by 15%, as compared to the clean Fe/W substrate.

EXPERIMENTAL RESULTS

In situ sample preparation and measurements were carried out at beamline D1011 of the MAX-Laboratory in Lund, Sweden. The base pressure of the joint analysis/preparation chamber was 10^{-10} mbar. Ultrathin bcc-Fe films of ∼3 ML were grown at room temperature onto a W(001) single crystal substrate using a mini e-beam evaporator. The samples were annealed at 460 °C to improve the structural quality of the Fe overlayers. Prior to Fe deposition, the W(001) single crystal substrate was cleaned by several oxidation and flash-annealing cycles. Oxidation of surface layers was carried out by annealing at 1000 °C for 10 min in 10^{-7} mbar oxygen. Subsequently, flash annealing to 1800 °C resulted in desorption of oxide layers and the recovery of a clean surface.[18]

The surface quality of the W(001) crystal and the pseudomorphic, epitaxial character of the bcc-Fe layers were monitored by low energy electron diffraction (LEED), as shown in Figure 2. A C_{60} layer of

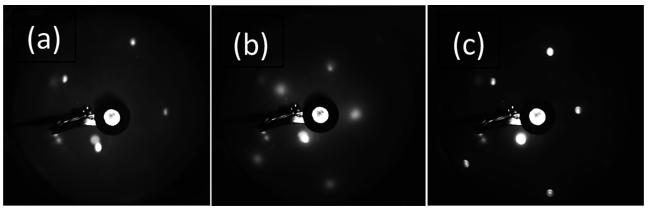

Figure 2. LEED patterns of (a) W(001) substrate, (b) as-grown ∼3 ML Fe on W(001), and (c) after annealing at 460 °C.

several nm thick was deposited onto the annealed Fe/W(001) samples by thermal evaporation using a custom-built Knudsen-cell. The LEED pattern of the single crystal W(001) substrate after cleaning showed a sharp (1 × 1) diffraction pattern. No additional features of super structures were observed, implying a high substrate quality.

The ultrathin Fe film on W(001) showed already a fairly high degree of structural order as-grown, which can be observed from the clear spots in the LEED pattern of Figure 2b. The crystallinity of the pseudomorphic Fe overlayers was further improved after annealing, resulting in the sharp LEED pattern of Figure 2c. In line with earlier observations of strain relief setting in at a coverage of about 5 ML,[18,19] we observed a slightly blurred LEED pattern for ∼6 ML Fe (not shown). In the following, we will focus on the results obtained for the Fe(3 ML)/W(001) sample.

In order to determine the Fe spin and orbital magnetic moments, we used XMCD.[31−34] We measured XMCD spectra at the Fe $L_{2,3}$ edges before and after C_{60} deposition and use the XMCD sum rules to calculate the spin and orbital magnetic moments.[33,34] The XAS spectra were measured at room temperature in the total electron yield (TEY) mode. The angle of incidence of the photon beam was set to 60° relative to the sample normal, while the degree of circular polarization was 75%. XMCD spectra were obtained in remanence, by taking the difference between the XAS spectra recorded with opposite in-plane magnetization directions.

The samples were magnetized by applying an in-plane magnetic field pulse of 300 Oe. The magnetic field was applied at an oblique in-plane angle, in between the ⟨110⟩ and ⟨100⟩ directions, i.e., neither along the magnetic easy axis nor along the hard axis.[18] In addition, the limited magnetic field strengths available at the beamline might be insufficient for saturating the magnetization of the films,[18] such that the remanent magnetization might be expected to be smaller than the saturation magnetization of the films. Hence, we expect that the magnetic moments extracted from the XMCD data using the sum rules are underestimated. However, this is of minor importance for the present study, since we are interested in relative changes to the moments induced by C_{60} adsorption.

Figure 3a shows the XAS and XMCD spectra, as well as the integrated XMCD intensity, recorded at the Fe $L_{2,3}$ edges for Fe(3

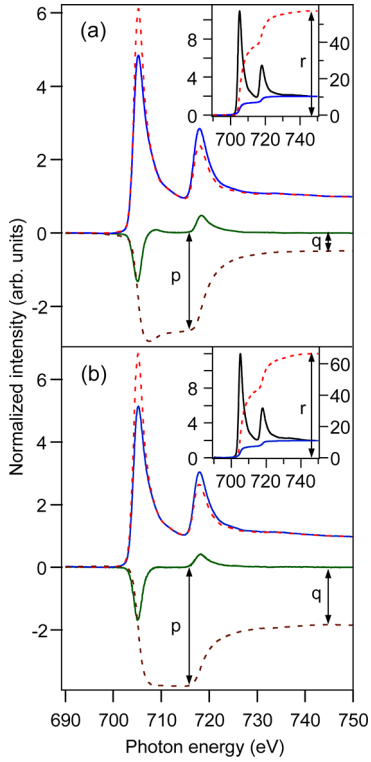

Figure 3. XAS spectra recorded at opposite remanent magnetization (red and blue) and the corresponding XMCD spectra (green) plus integrated XMCD intensity (brown) at the Fe $L_{2,3}$ edges, of (a) 3MLs of Fe on W(001) and (b) the same sample after deposition of several nm of C_{60}. The XAS spectra were normalized on the step height above 740 eV photon energy, where dichroic effects are absent. Insets show the summed XAS spectra and their integrals. A stepped background (blue) was subtracted from the summed XAS spectra prior to integration, following the procedure developed by Chen et al.[31]

ML)/W(001). The inset shows the sum of the XAS spectra recorded with opposite photon helicity and its integral. The XMCD spectra have been corrected by taking into account the incident angle (30° with respect to the sample surface) and the degree of circular polarization (75%), by multiplying the measured spectra by [1/cos(30°)]/0.75, while keeping the sum spectra the same.[31] Using the established sum rules,[33,34] we obtain the spin and orbital magnetic moments, μ_S and μ_L, from the integrals of the XAS and XMCD spectra as[31,33,34]

$$\mu_S = -\frac{6p - 4q}{r} n_h, \qquad \mu_L = -\frac{4q}{3r} n_h \tag{1}$$

Here, n_h is the number of holes, where we use $n_h = 3.39$.[31] The quantities p, q, and r are indicated in Figure 3. The small term proportional to the expectation value of the magnetic dipole operator was neglected in the determination of μ_S.[31] The values we obtain for the Fe(3 ML)/W(001) sample are $\mu_S = 0.83\ \mu_B$ and $\mu_L = 0.038\ \mu_B$.

These values are considerably smaller than the saturation values for Fe, as expected (see discussion above). It should be noted in passing that $\mu_L/\mu_S = 0.046$, which is only slightly higher than the bulk value of 0.043.[31] This is somewhat surprising, since for ultrathin 3d transition metal films, this ratio is typically enhanced, due to film−substrate *d-orbital* interaction and lifting of the orbital degeneracy by symmetry reduction at the surface.[28−32] In this respect, the magnetic properties of the Fe/W(001) interface are somewhat special.

The XAS and XMCD spectra recorded at the Fe $L_{2,3}$ edge of the Fe/W(001) sample, covered by a C_{60} overlayer of several nm thick, are

dx.doi.org/10.1021/am3024367 | ACS Appl. Mater. Interfaces 2013, 5, 837−841

shown in Figure 3b. Using eq 1, we obtain $\mu_S = 0.78\ \mu_B$ and $\mu_L = 0.126\ \mu_B$, leading to a ratio $\mu_L/\mu_S = 0.161$. Compared to the results obtained for the clean Fe/W(001) substrate, μ_S is reduced by 6%, whereas the μ_L/μ_S ratio is strongly increased by 250%. Enhanced orbital moments of 3d transition metal systems typically originate from an increased degree of 3d wave function localization (see, for example, ref 23), which in the present case should result from hybridization between the Fe 3d states and the C_{60} orbitals.

DISCUSSION

The relative changes in μ_S upon adsorption of C_{60}, extracted from the experiment and from the calculations, agree quite well. The interfacial bonding between the Fe surface and the C_{60} molecules results from hybridization between the 3d orbitals of the Fe surface atoms and the frontier π orbitals of C_{60}, which we have previously observed using C K-edge XAS and XMCD measurements.[15] The hybrid interface states have metallic character, and they give rise to a magnetic moment $\mu_S = -0.21$ and $-0.27\ \mu_B$ on the C_{60} molecule for adsorption on Fe(001) and Fe/W(001), respectively. This moment is antiferromagnetically ordered with respect to those of the Fe substrate atoms, as are the moments on the W atoms in the Fe/W substrate; see Figure 1a. The magnitude and sign of the spin polarization of C_{60}-derived states depends strongly on binding energy, in agreement with experiments.[15] Close to the Fermi energy (within plus or minus 0.5 eV), the maximum value reached is about 2:1 (minority/majority spin DOS of occupied orbitals).

The effect of hybridization on the Fe surface can be analyzed using the projected density of states (PDOS), as shown in Figure 4. Compared to the top layer of the clean Fe(001) surface, the PDOS of the Fe interface layer of the C_{60}/Fe(001) system is slightly decreased (increased) for majority (minority) spin below the Fermi level; see Figure 4a, consistent with a reduced spin polarization. These changes are not homogeneous in the Fe(001) plane, as only part of the Fe atoms bind to C_{60} directly. Figure 4b shows the PDOS projected on a Fe atom that is strongly bonded to C_{60} (the atom marked red in Figure 1b), compared to a surface atom on the clean Fe(001) surface.

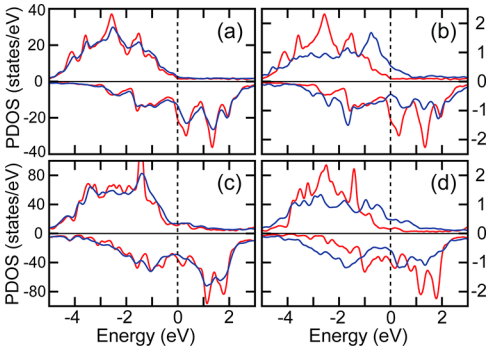

Figure 4. (a) PDOS of majority (top) and minority (bottom) spin states projected on the top Fe layer at the C_{60}/Fe(001) interface (blue), compared to the PDOS of a clean Fe(001) surface layer (red); (b) PDOS of the most strongly affected Fe atom (blue), compared to the PDOS of a clean Fe(001) surface atom; (c,d) as (a,b), but for the Fe/W(001) substrate.

The minority spin PDOS of the clean Fe(001) surface just above the Fermi level is dominated by peaks resulting from *d-states* that have a large amplitude (or are even localized) at the surface. Upon adsorption of C_{60}, these peaks are suppressed, as the corresponding states participate in the bonding to the adsorbate. In Figure 4b, hybrid bonding states appear in the minority spin channel at an energy of ~−2 to −4 eV. Concurrently, the majority spin PDOS in the latter energy region is reduced by bonding to the adsorbate, and an antibonding hybrid state appears just below the Fermi energy. These changes lead to a strongly reduced magnetic moment on this particular Fe atom, as discussed above.

Figure 4c shows the PDOS projected on the three Fe layers of the Fe/W(001) system before (red) and after (blue) adsorption of C_{60}. In detail, the PDOS is different from that of the pure Fe substrate, Figure 4a, but the overall trend is the same; adsorption of C_{60} decreases (increases) the majority (minority) spin PDOS of the occupied states. Projecting on a Fe atom strongly involved in bonding to C_{60} (the atom marked red in Figure 1a) gives the PDOS shown in Figure 4d. The pattern is quite comparable to that observed for the pure Fe substrate in Figure 4b. The similarity between the C_{60}/Fe(001) and C_{60}/Fe/W(001) systems is quite remarkable, in view of the structural differences between the two substrates before and after adsorption of C_{60}. One can conclude that such structural differences are not so important for the magnetic and electronic properties of these systems.

CONCLUSIONS

By a joint computational and experimental approach, we have characterized well-defined interfaces between C_{60} molecules and Fe(001) surfaces, which have high relevance for organic spintronics. Hybridization between the frontier orbitals of C_{60} and Fe 3d states has a strong effect on the spin polarization of the interface, which underlines the potential of chemical tuning of OSC/FM "spinterfaces" for spintronic devices.

Our calculations show that the hybrid interface states lead to magnetic moments on the C_{60} molecules that are coupled antiparallel to the Fe moments: $\mu_S = -0.21$ and $-0.27\ \mu_B$ per molecule for adsorption on Fe(001) and Fe/W(001), respectively. The moments of the Fe atoms at the interface are also affected significantly. XMCD experiments of 3 MLs of Fe on W(001) show that the overall Fe spin moment is reduced by 6% after adsorption of C_{60}. This is in good agreement with the calculated values for both C_{60}/Fe(001) and C_{60}/Fe/W(001), which show a similar spin dependent electronic structure at the hybrid interfaces, in spite of their significant structural differences. It should be noted, however, that a direct comparison of the reduction of the magnetic moments obtained from experiments and calculations should be made with care, since the effects are far from homogeneous.

AUTHOR INFORMATION

Corresponding Author

*E-mail: m.p.dejong@utwente.nl.

Notes

The authors declare no competing financial interest.

ACKNOWLEDGMENTS

The authors acknowledge support from the European project MINOTOR (Grant No. FP7-NMP-228424), the European Research Council (ERC Starting Grant No. 280020), and the NWO VIDI program (Grant No. 10246). The use of supercomputer facilities was sponsored by the "Stichting Nationale Computerfaciliteiten (NCF)", financially supported

by the "Nederlandse Organisatie voor Wetenschappelijk Onderzoek (NWO)".

REFERENCES

(1) Naber, W. J. M.; Faez, S.; van der Wiel, W. G. *J. Phys. D: Appl. Phys.* **2007**, *40*, R205−R228.
(2) Dediu, V. A.; Hueso, L. E.; Bergenti, I.; Taliani, C. *Nat. Mater.* **2009**, *8*, 707−716.
(3) Žutić, I.; Fabian, J.; Das Sarma, S. *Rev. Mod. Phys.* **2004**, *76*, 323−410.
(4) Santos, T. S.; Lee, J. S.; Migdal, P.; Lekshmi, I. C.; Satpati, B.; Moodera, J. S. *Phys. Rev. Lett.* **2007**, *98*, 016601.
(5) Barraud, C.; Seneor, P.; Mattana, R.; Fusil, S.; Bouzehouane, K.; Deranlot, C.; Graziosi, P.; Hueso, L.; Bergenti, I.; Dediu, V.; Petroff, F.; Fert, A. *Nat. Phys.* **2010**, *6*, 615−620.
(6) Tran, T. L. A.; Le, T. Q.; Sanderink, J. G. M.; van der Wiel, W. G.; de Jong, M. P. *Adv. Funct. Mater.* **2012**, *22*, 1180−1189.
(7) Xiong, Z. H.; Wu, D.; Vardeny, Z. V.; Shi, J. *Nature* **2004**, *427*, 821−824.
(8) Dediu, V.; Hueso, L. E.; Bergenti, I.; Riminucci, A.; Borgatti, F.; Graziosi, P.; Newby, C.; Casoli, F.; de Jong, M. P.; Taliani, C.; Zhan, Y. *Phys. Rev. B* **2008**, *78*, 115203.
(9) Schoonus, J. J. H. M.; Lumens, P. G. E.; Wagemans, W.; Kohlhepp, J. T.; Bobbert, P. A.; Swagten, H. J. M.; Koopmans, B. *Phys. Rev. Lett.* **2008**, *103*, 146601.
(10) Gobbi, M.; Golmar, F.; Llopis, R.; Casanova, F.; Hueso, L. E. *Adv. Mater.* **2011**, *23*, 1609−1613.
(11) Lin, R.; Wang, F.; Wohlgenannt, M.; He, C.; Zhai, X.; Suzuki, Y. *Synth. Met.* **2011**, *161*, 553−557.
(12) Gobbi, M.; Golmar, F.; Llopis, R.; Casanova, F.; Hueso, L. E. *Org. Electron.* **2012**, *13*, 366−372.
(13) Sanvito, S. *Nat. Phys.* **2010**, *6*, 562−564.
(14) Schmaus, S.; Bagrets, A.; Nahas, Y.; Yamada, T. K.; Bork, A.; Bowen, M.; Beaurepaire, E.; Evers, F.; Wulfhekel, W. *Nat. Nanotechnol.* **2011**, *6*, 185−189.
(15) Tran, T. L. A.; Wong, P. K. J.; de Jong, M. P.; van der Wiel, W. G.; Zhan, Y. Q.; Fahlman, M. *Appl. Phys. Lett.* **2011**, *98*, 222505.
(16) Kawahara, S. L.; Lagoute, J.; Repain, V.; Chacon, C.; Girard, Y.; Rousset, S.; Smogunov, A.; Barreteau, C. *Nano Lett.* **2012**, *12*, 4558−4563.
(17) Jones, T. L.; Venus, D. *Surf. Sci.* **1994**, *302*, 126−140.
(18) Wulfhekel, W.; Zavaliche, F.; Hertel, R.; Bodea, S.; Steierl, G.; Liu, G.; Kirschner, J.; Oepen, H. P. *Phys. Rev. B* **2003**, *68*, 144416.
(19) von Bergmann, K.; Wiesendanger, R. *Phys. Rev. B* **2004**, *70*, 174455.
(20) Spišák, D.; Hafner, J. *Phys. Rev. B* **2004**, *70*, 195426.
(21) Kubetzka, A.; Ferriani, P.; Bode, M.; Heinze, S.; Bihlmayer, G.; von Bergmann, K.; Pietsch, O.; Blügel, S.; Wiesendanger, R. *Phys. Rev. Lett.* **2005**, *94*, 087204.
(22) Blöchl, P. E. *Phys. Rev. B* **1994**, *50*, 17953−17979.
(23) Kresse, G.; Joubert, D. *Phys. Rev. B* **1999**, *59*, 1758−1775.
(24) Kresse, G.; Hafner, J. *Phys. Rev. B* **1993**, *47*, 558−561.
(25) Kresse, G.; Furthmüller, J. *Phys. Rev. B* **1996**, *54*, 11169−11186.
(26) Perdew, J. P.; Burke, K.; Ernzerhof, M. *Phys. Rev. Lett.* **1996**, *77*, 3865−3868.
(27) Kittel, C. *Introduction to Solid State Physics*; Wiley: New York, 1996; p 23, 449.
(28) Ferriani, P.; Heinze, S.; Blügel, S. *Phys. Rev. B* **2005**, *72*, 024452.
(29) Li, H. I.; Pussi, K.; Hanna, K. J.; Wang, L.-L.; Johnson, D. D.; Cheng, H.-P.; Shin, H.; Curtarolo, S.; Moritz, W.; Smerdon, J. A.; McGrath, R.; Diehl, R. D. *Phys. Rev. Lett.* **2009**, *103*, 056101.
(30) Shi, X.-Q.; Hove, M. A. V.; Zhang, R.-Q. *Phys. Rev. B* **2012**, *85*, 075421.
(31) Chen, C. T.; Idzerda, Y. U.; Lin, H. J.; Smith, N. V.; Meigs, G.; Chaban, E.; Ho, G. H.; Pellegrin, E.; Sette, F. *Phys. Rev. Lett.* **1995**, *75*, 152−155.
(32) van der Laan, G. *Phys. Rev. Lett.* **1999**, *82*, 640−643.
(33) Carra, P.; Thole, B. T.; Altarelli, M.; Wang, X. D. *Phys. Rev. Lett.* **1993**, *70*, 694−697.
(34) Thole, B. T.; Carra, P.; Sette, F.; van der Laan, G. *Phys. Rev. Lett.* **1992**, *68*, 1943−1946.